Original

Tracking Technique of a Micro Guide Wire in Sequential Fluorograms

AKIHIRO TAKEMURA, MASAYUKI SUZUKI, HAJIME HARAUCHI[1] and YUSUKE OKUMURA[2]

Division of Health Sciences, Graduate School of Medical Science, Kanazawa University
1)Department of Radiological Technology, Kawasaki College of Allied Health Professions
2)Department of Radiology, Ishikawa Saiseikai Kanazawa Hospital

Received July 8, 2005
Revision accepted Oct. 18, 2005
Code No. 532

Introduction

Three-dimensional (3D) information is useful in medical situations. Multislice-computed tomography systems have made it possible to acquire long-range volume data and/or isotropic volume data, and many angiography systems can now build 3D images from rotational angiography.[1]

In vascular intervention (IVR), devices such as guide wires, catheters, and coils are used. 3D positional information of these devices can help radiologists to facilitate IVR,[2] especially IVR of cerebral artery diseases like aneurisms and arteriovenous malformations (AVMs) because of the complex artery tree structure and the risks of critical side effects from incorrect catheterizations.

Several image-based techniques have been proposed. Some of them produce the 3D positional information of guide wires from a single plane image or biplane images,[3-5] while another is a technique for micro catheters combined with preoperative magnetic resonance angiography volume data.[6] However, all of these techniques require manual interaction to indicate such devices.

In the IVR of cerebral arteries, an automatic tracking technique for micro guide wires should be required because micro guide wires are used to lead a micro catheter into aneurysms or AVMs. Several studies of automatic tracking techniques for guide wires in fluorograms have been published,[7-10] but they may apply only to guide wires and not to micro guide wires.

A tracking technique for micro guide wires can also enhance them in fluoroscopy for display. Micro guide

Summary

In this paper, we propose a tracking technique for a micro guide wire in a sequence of fluorograms. A technique in which the region-growing technique was embedded was developed. It gives the center line of a micro guide wire. A sequence of 1,024×1,024×16 bit fluorograms (111 frames) with a carotid phantom and head phantom was obtained with a CAS-8000V (Toshiba America Medical Systems, Inc., CA, USA) C-arm angiography system and a Hi-Torque Standard micro guide wire (Advanced Cardiovascular Systems, Inc., CA, USA). To evaluate the technique, we manually traced the guide wire in each sequence frame three times, and a "true" single-width micro guide wire was created from them. The number of pixels on the true guide wire and inside the two-pixel tolerance of the center line was counted in each fluorogram, and the percentage of that count based on the number of all pixels on the true guide wire was calculated as true positive (TP). In addition, the number of pixels on the center line and outside the two-pixel tolerance of the true guide wire was counted in each frame as false positive (FP). The tracking technique has a mean TP of 94.8% and a mean FP of 5.1 pixels/frame. Several frames have low TP and high FP, but the technique could continue to track the micro guide wire until the end of the sequence. We therefore concluded that we had developed an accurate automatic tracking technique for micro guide wires in fluoroscopic sequences.

Key words: Guide wire tracking, Fluorography, Micro guide wire, Vascular intervention, Region growing

別刷資料請求先：〒920-0942 石川県金沢市小立野5-11-80
金沢大学医学系研究科保健学専攻量子医療技術学講座 武村哲浩 宛

wires in fluoroscopic images are not easily identified because fluoroscopic images are usually noisy and the micro guide wires in these images are thin.

In this paper we propose a tracking technique for a micro guide wire in sequential fluorograms.

1. Methods

A schema of the tracking technique we developed is shown in Fig. 1. It requires only the initial position of the micro guide wire in the first frame to start tracking. First, a fluorogram is filtered by a 3×3 average filter to reduce image noise, and the region-growing technique then extracts rough guide wire regions. The double-ring tracking proceeds to trace the curvature of regions by using the two profiles on the rings and represents some of the tree structures along the regions. Unwanted branches in the tree structures, e.g., those produced by bone edges, are killed, and the longest polygonal line is chosen. It is interpolated by the spline interpolation, and the spline curvature is then created. It is taken as the center line of a micro guide wire. If the sequence has subsequent frames, the positions of the pixels on the curvature are used as start points for the region-growing process in the next frame.

A sequence of 111 fluorograms (1,024×1,024×16 bits) was obtained using a CAS-8000V (Toshiba America Medical Systems Inc., CA, USA) C-arm angiography system as a Hi-Torque Standard (Advanced Cardiovascular Systems, Inc., CA, USA) micro guide wire was passed through a carotid phantom, which was on top of a head phantom. The sequence was acquired at 30 frames/sec using pulsed fluoroscopy at 94 kV and 50 mA (pulse width=3.2 msec). This exposure condition was automatically determined by the angiography system. It enabled us to obtain the same quality images as clinical images. The 7-inch image-intensifier mode was used (pixel size=0.174 mm). The source-to-image distance was 100 cm, and the magnification was 1.35 times at the table-top (Fig. 2a). The carotid phantom was a silicone cylinder containing a simulated vessel with the shape and curvatures of the internal carotid artery from just above the carotid bifurcation up to the circle of Willis (Fig. 2b). The vessel in the carotid phantom was filled with a glycerin-water solution. The head phantom (Fig. 2c) consisted of a human skull, and tissue-equivalent material and was used to provide the bony background in the fluorographic images. After acquisition, the sequence was transferred to the computer for analysis. The mean standard deviation (SD) of pixel intensity of the background around the micro guide wire tip in the fluorograms was 60.1, and its mean signal-to-noise ratio was 1.67. It was used for the development of this technique and for evaluation.

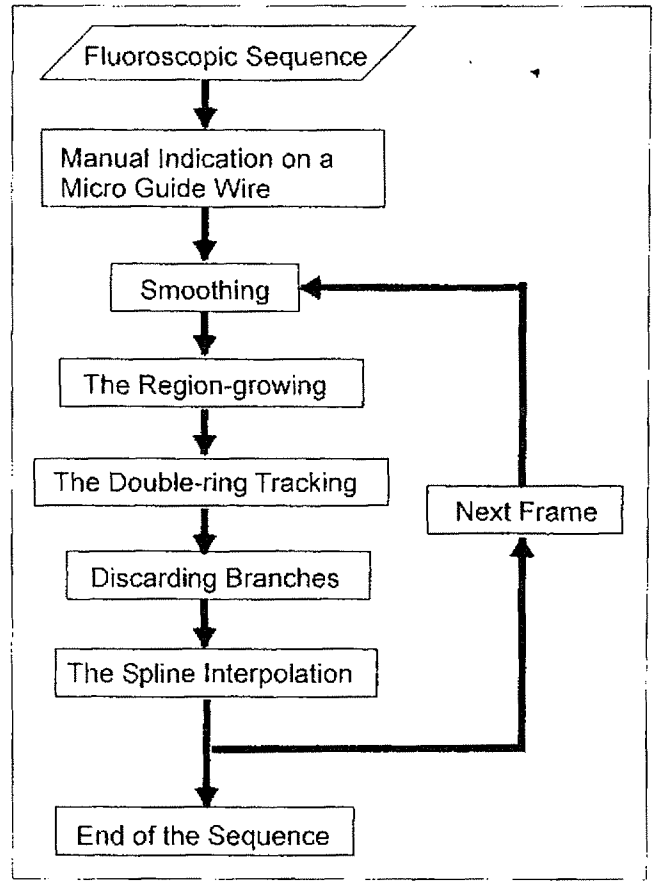

Fig. 1 Schema of the micro guide wire tracking method.

1-1 Initial extraction by the region-growing technique

The region-growing technique is an extraction method in which a measure is calculated from neighbor pixels around a focused pixel, and its process is spread from the focused pixel to its neighbors.[11-14] The initial focused points (seed points) are usually indicated manually. The variance and mean of intensities of the focused pixel and its neighbors are frequently used to calculate a measure, or either of them is itself a measure.

Micro guide wires in fluorograms have almost the same signal intensity as the bony background, and variance of the intensities of the pixel on the micro guide wire and its neighbors is just slightly higher than that of the background. Thus these values are not suitable for the measure in our region-growing process. The difference between micro guide wires and the bony background should be only that the micro guide wires have

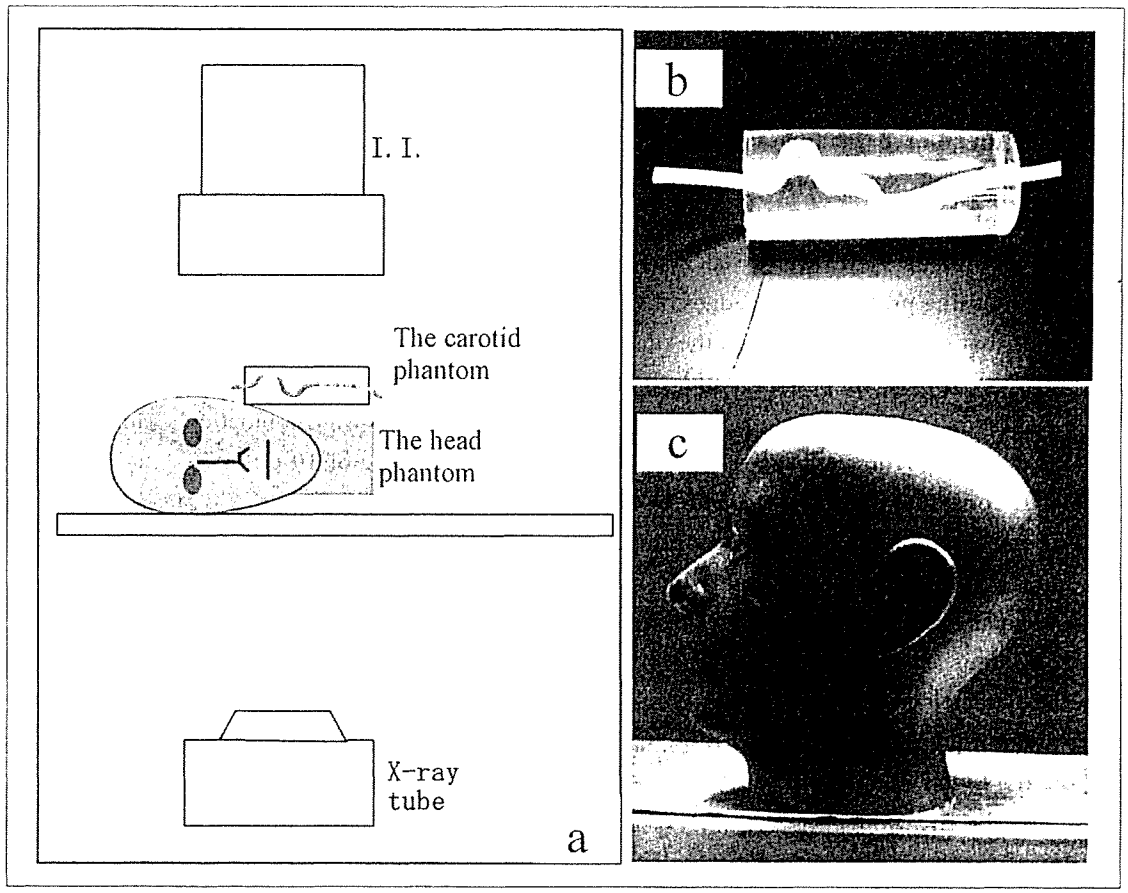

Fig. 2 Phantoms and settings for acquisition of the fluorographic images. Image (a) illustrates the configuration of the locations of the head phantom, tube phantom, image-intensifier (I.I.), and X-ray tube in the experiment. Image (b) is the tube phantom, which was a simulated curvature of a typical carotid artery and was fixed in a silicone cylinder. Image (c) is the head phantom that was used with the intention of adding bony background to the fluorographic images.

uniform width curvatures.

For these reasons, we employed a measure obtained from the convolution of a second derivative filter and the same size region in the original images centered on the focused pixel. The filter kernel is defined as

$$K_{m\times m}(u,v)=\begin{cases}1 & when\ u=0,\ u=m-1,\ v=0,\ or\ vv=m-1\\ -4(m-1) & when\ the\ center\ of\ kernel\\ 0 & otherwise\end{cases} \quad \cdots\cdots(1)$$

where, $K_{m\times m}(u, v)$ means an $m\times m$ filter kernel, and u and v are coordinates in the kernel.

And the measure value $C(x, y)$ is calculated as

$$C(x,y)=\sum_{y=0}^{m-1}\sum_{x=0}^{m-1}K_{m\times m}(u,v)\cdot R_{m\times m}(x+u-\frac{1}{2},\ y+v-\frac{m}{2}) \quad \cdots\cdots(2)$$

where $R_{m\times m}(x, y)$ means an $m\times m$ region centered on a focused pixel (x, y) in the fluorogram. According to the change in m dependent on the width of the micro guide wires, it could adapt to any guide wire size. To get the best size m for our micro guide wires, we tried 5×5 to 13×13 kernel sizes and found that the 9×9 kernel was the best for the micro guide wires in our fluorograms.

A seed point must be indicated manually only in the initial frame, and in the subsequent frame the pixels of the curvature of a guide wire center line determined in the previous frame is taken as seed points.

Once the seed point is indicated, the threshold value for C, which judges the extraction of the pixel, is calculated. The mean and SD of the measure values C for all pixels in the 41×41 region centered on the seed point are calculated, and the threshold for C is then determined along the mean value plus twice the SD. If C for a focused pixel is larger than the threshold value, the pixel will be extracted. At this point, a binary image of the extracted guide wire is obtained.

The mean plus twice the SD was chosen by means of the results for the mean plus the SD to the mean plus three times the SD. The 41×41 region was the minimum size needed to produce almost the same mean and variance as the background.

1-2 Double-ring tracking

This process traces the regions extracted by the region-growing process at a constant interval and provides nodes of a tree structure for the following processes "discarding branches and the spline interpolation." Profiles on double rings are used to determine the direction of the next position. Hoffmann et al.[15] proposed a vessel-tracking technique by using profiles on the edges of two boxes. The yield of that tracking depends on the direction of the vessels, i.e., if they are perpendicular to the box edges, the yield is half the edge length, but if they slant, the yield is the square root of 2 times that length at the maximum. A constant yielding is needed for our technique to kill unwanted branches in a tree structure (see next section). For that reason, we used two rings. It yields a distance equal to the radius of the outside circle.

The following steps are performed in this process: first, a pixel of the extracted binary guide wire is searched by using raster scanning. When a guide wire pixel is encountered, the tracking of an extracted region starts at that position i.e., the first node.

The profiles of pixel intensities on the two different radius rings centered on the first node position are obtained (Fig. 3). They shows pixel values as a function of angles and have only two values, 0 (background) or 1 (extracted region), since the image after the region-growing process is a binary image. The coordinate system of the profiles is matched to that of the image in the case of the first node. In the other cases, the Y-axis of the coordinate system is set to a vector from the current node to the previous one, and the X-axis is orthogonal to the vector.

The two binary profiles are performed logical AND operation each other, and the resultant profile is obtained. Ranges of angle that have the value 1 (i.e., extracted region) are searched for in the profile. The two widest-angle ranges are selected if three or more ranges are available. The angle at the midpoint of the angle range is a direction toward the next node, which is located on the intersection of the direction and the outside ring. After determination of the next node (s) at the current position, the inside of the inner ring is filled with 0 (background) to prevent trace-back. If there is only one angle range, that means that the current tracking position is on the body of the guide wire; if there are two ranges, it is on the bifurcation; and if there is no range, it is on the terminal.

When a series of region tracking reaches the end, raster scanning is continued to find another remaining extracted region. The end of raster scanning is the end of this process.

The use of double-ring profiles prevents region tracking from jumping into another branch. In other words, it has the effect of correctly finding bifurcation points. The best diameters of two rings depend upon the widths of micro guide wires in fluoroscopic images. We tried combinations of the diameters of 7 to 13 pixels for the inner ring and of 15 to 27 pixels for the outer ring. As a result, we chose a combination of an inner ring of 9 pixels and outer ring of 19 pixels.

1-3 Discarding branches and the spline interpolation

The discrete nodes given from the double-ring tracking process could be a tree structure having branches; thus, unwanted branches produced by background, such as bone edges, must be killed.

This process follows the nodes of a tree structure from all terminals and chooses two longer branches to a bifurcation point. In the images from which the guide wires were extracted, the unwanted branches would be sufficiently shorter than the main branch (the guide wire). In the case of a tree structure produced from a region in Fig. 3, for example, it has three terminals and one bifurcation. The number of nodes from each terminal to the bifurcation node is counted, the shortest branch is killed, and one polygonal line will ultimately be obtained.

The nodes of the polygonal line are interpolated by the spline interpolation. The spline curvature is a center line of the micro guide wire.

1-4 Evaluation

To evaluate the technique, we created the "true" single-pixel-width micro guide wire. The guide wire in each image of the sequence was manually traced three times by single-pixel-width curvature, and three binary images of the micro guide wire were obtained. The "true" micro guide wire image was created from the three binary micro guide wire images by the following logical operations as

$$\left.\begin{aligned} G_{1and2} &= G_1 \; AND \; G_2 \\ G_{1or2} &= G_1 \; OR \; G_2 \\ G_{1or2and3} &= G_{1or2} \; AND \; G_3 \\ G_{truth} &= G_{1or2and3} \; OR \; G_{1and2} \end{aligned}\right\} \quad \cdots\cdots\cdots\cdots\cdots\cdots (3)$$

where G_1, G_2, and G_3 are the manually traced images and G_{truth} is the true image. The guide wire in G_{truth} was sometimes separated into two or more segments of curvatures

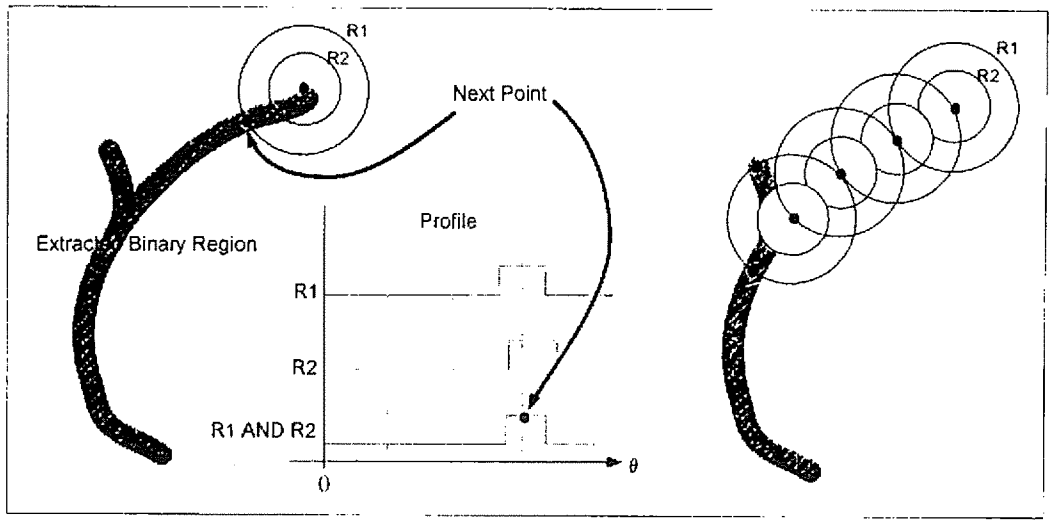

Fig. 3 Double-ring tracking.
Two profiles that are functions of angles on the two rings are obtained, and the next position(s) will be determined according to the profiles resulted by the AND operation of the two profiles. After that the inner ring area is filled with 0 (background).

after the logical operations. The separated segments were connected manually to each other.

We calculated true and false positives by using the true micro guide wires to evaluate the accuracy of our technique. The number of pixels on the true guide wire and inside the two-pixel tolerance of the center line obtained by our technique was counted in each fluorogram, and then the percentage of that count based on the number of all pixels on the true guide wire was calculated as true positive (TP) (Fig. 4a). Also, the number of pixels on the center line and outside the two-pixel tolerance of the true guide wire was counted in each frame as false positive (FP) (Fig. 4b). Two-pixel-width tolerance was chosen because the width of the micro guide wires in the fluorograms was almost five pixels.

Studies about segmentation, such as the paper written by Hayashi et al,[16] have used correct and wrong percentages based on the area of both true and segmented regions to evaluate precision. In the end, our technique gives a single-pixel-width curvature, not a region. Thus, that percentage value could not correctly evaluate the accuracy of our technique. Our respective definitions of TP and FP are the number of signals our technique obtained correctly and the number of wrong pixels it took, like in a basic 2×2 decision matrix of receiver operating characteristic (ROC) analysis.

2. Results

The TP and FP in each frame are shown in Fig. 5. Mean TP and mean FP were 94.8% and 5.1 pixels per frame, respectively. The higher FPs and lower TPs were obtained at about frame 30 through frame 40. However, the tracking continued to follow the motion of the micro guide wire until the sequence ended.

The number of frames in which the tracking technique resulted in TPs larger than 90% was 92 (82.9%) frames. The number of frames in which the tracking technique resulted in FPs with fewer than 15 pixels was 100 (90.1%) frames. The true micro guide wire in each frame was constant at about 150 pixels.

Three frames of the original images on which the resultant curvatures were superimposed are shown in Fig. 6 as examples of the resultant images. These images are frames in the beginning, middle, and end of the sequence.

3. Discussion

We can say that these results are good: a mean TP of 94.8%; mean FP of 5.1 pixels per frame; 92 frames (82.9%) with TP more than 90%; and 100 frames (90.1%) with FPs fewer than 15 pixels per frame. A TP of about 95% means that only seven or eight pixels of the true guide wire were left, and they were equal to about 1.4 mm in length in the image. An FP of 5 pixels per frame also means that 0.87 mm of the full length of an identified guide wire was wrong. Additionally, it is important that the tracking technique could follow the guide wire until the end of the sequence.

The FPs for frames 30 through 40 were higher than those for the other frames, and the highest was 40 pixels per frame. These FPs were caused by overidenti-

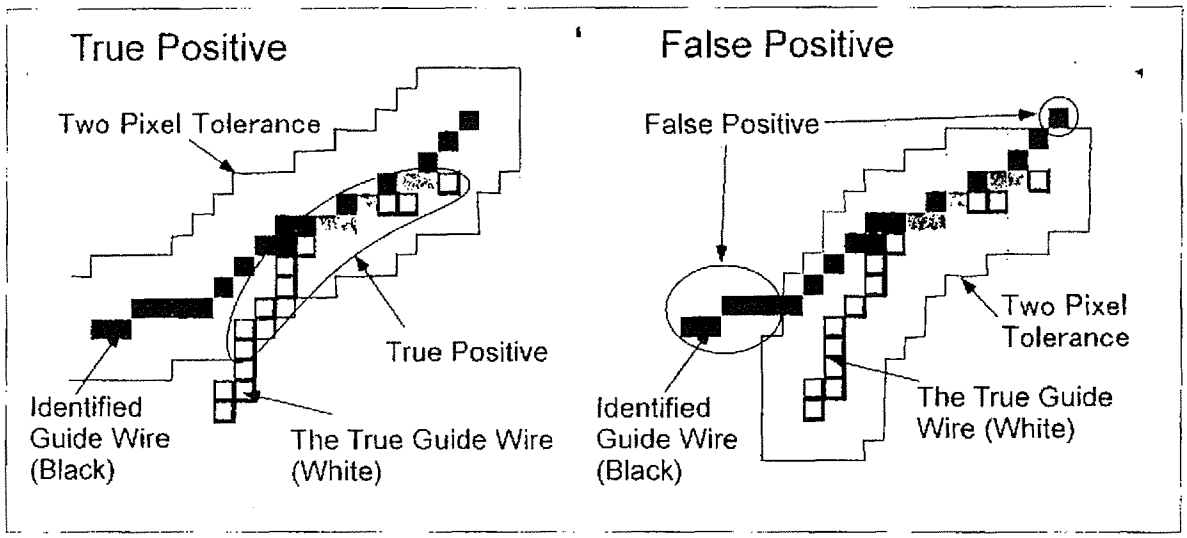

Fig. 4 True positive and false positive.
Image (a) illustrates true positive (TP), and image (b) illustrates false positive (FP). TP is the percentage of pixels of true micro guide wire inside the two-pixel tolerance of an identified micro guide wire based on the number of all pixels of the true micro guide wire. FP is the number of pixels outside the two-pixel tolerance of true micro guide wire.

a | b

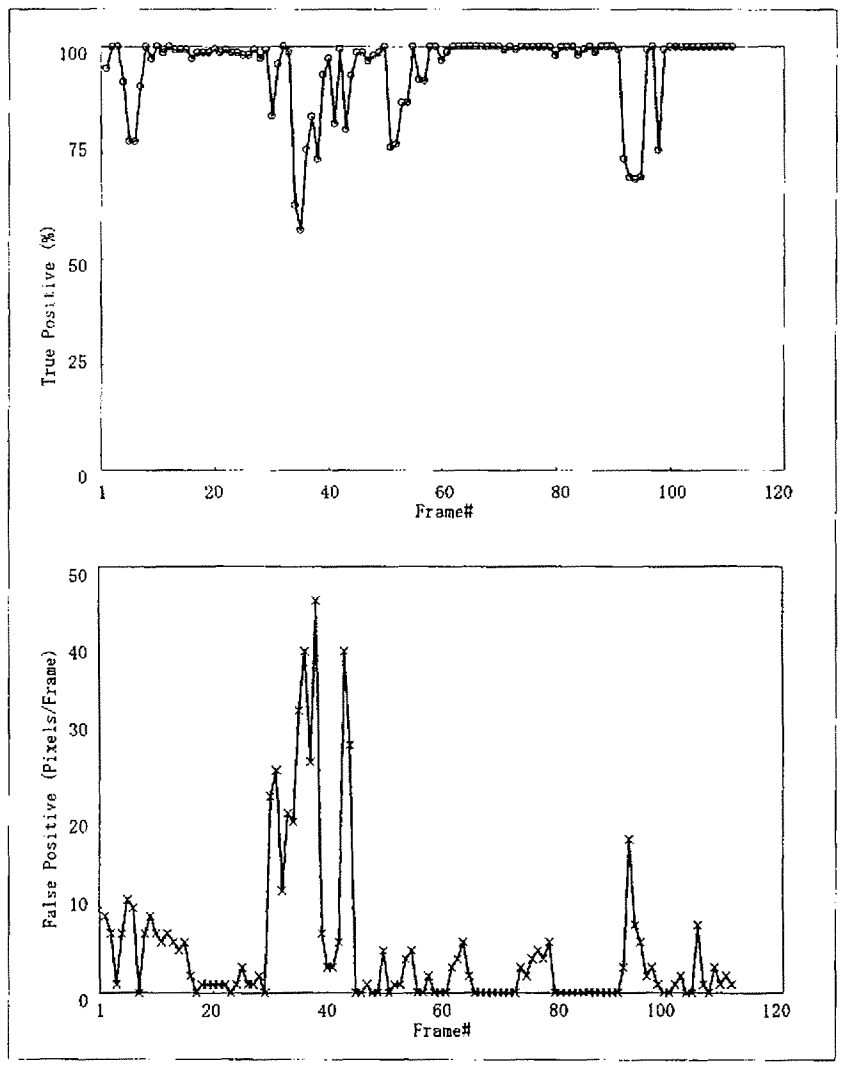

Fig. 5 Results of true positive and false positive in each frame. The graph (a) shows the true positive values as a function of frame number, and the graph (b) shows the false positive values as a function of frame number.

a
b

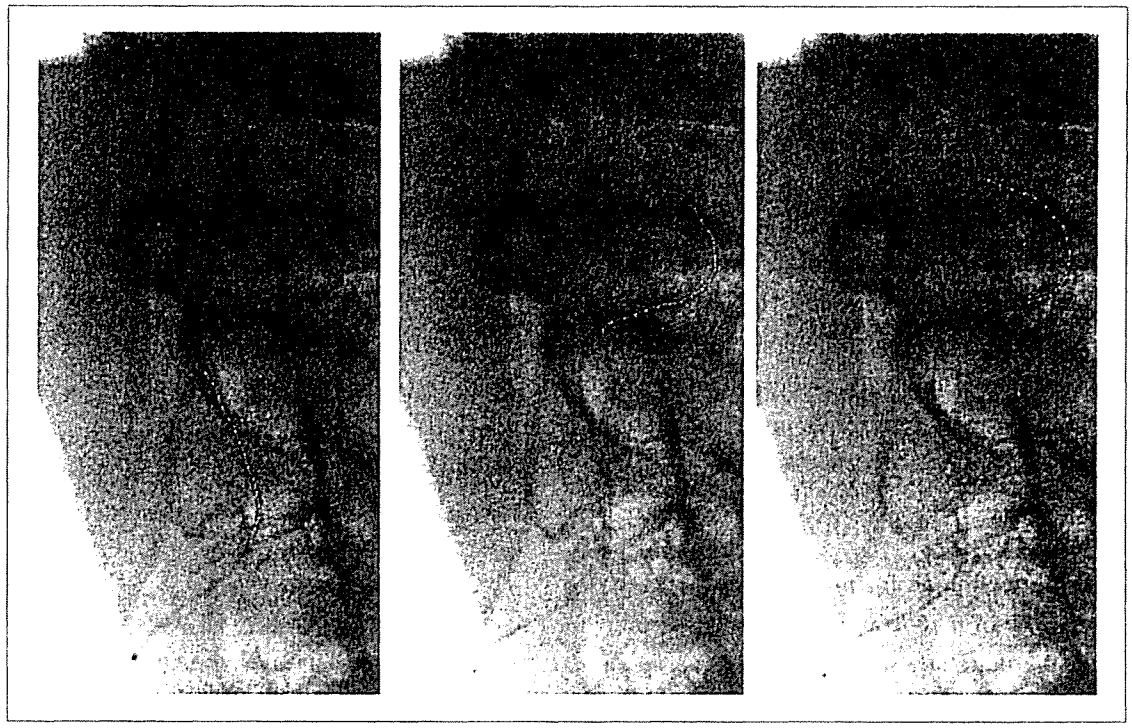

Fig. 6 Examples of the resultant micro guide wires that were superimposed onto a part of the original fluoroscopic images. The white dots in these images are nodes of the tree structures that resulted from the double-ring tracking. The gray curvatures are the final identified micro guide wires.

fication of the micro guide wire lead part. Micro guide wires have a radio-opaque part at the distal end following the section of lead wire. The lead wire part is usually less radio-opaque than the radio-opaque distal part, but it is a part of the micro guide wire. Our tracking technique identified the lead part of the guide wire in those frames; thus the FP values worsened. However, although it had a mean FP of 5 pixels per frame, that means that only about 3% of the identified micro guide wire was wrong, which is not a bad result. An example of the frames is shown in Fig. 7.

Images of 1,024×1,024 are required for this technique. The width of the micro guide wire in this sequence was about 5 pixels. This means that 512×512 images will show a guide wire width of 2.5 pixels. If thinner guide wires are represented under lower magnifications, they can hardly be detected and tracked in 512×512 images.

Sequential fluorograms of four seconds were used to evaluate this technique. This does not mean that our technique can process only four-second fluorography. The technique can deal with any duration of fluorography.

This technique should be improved for real-time execution since the technique took about 42 seconds with a personal computer (CPU: Pentium4 2.4 GHz) to track a micro guide wire in the 111 images. The reason is not only the algorithm but also transferring the image data to an external hard disk. Each image had to be read one by one from the hard disk, a process that took time. Our eventual aim is that image data will be transferred directly to the computer's memory from the angiography system, without having to go through a hard disk.

We used the fluoroscopic images of the phantom experiment because it is difficult to obtain sequences of clinical fluoroscopic images. Many angiography systems can store a fluoroscopic sequence temporarily, but they cannot store it on a hard disk drive. This means that it is necessary to interrupt the IVR operation to obtain clinical fluoroscopic images.

We think our tracking technique has the potential to be used in clinical situations. The difference between clinical fluoroscopic images and the fluoroscopic images of the phantom experiment likely would be minor. The fluoroscopic images we obtained have the same bony background as clinical images. Although we used a carotid phantom, the phantom would increase in quantum noise to the region of the image. In other words, it would make the identification of guide wires more difficult, but our technique was able to provide accurate tracking.

A limitation of our study design is that only phan-

tom images were employed for evaluation of the performance of our tracking technique. A phantom experiment would reveal the maximum performance of our technique. Signal intensities and image noise in clinical fluoroscopic images depend on many factors, including the patient, X-ray exposure conditions, and micro guide wire. Thus this tracking technique should be assessed with several clinical sequences. However, there are many problems remaining to be solved to obtain clinical fluorographic sequences, as described above. Therefore, the assessment of clinical images is one of our future goals.

4. Conclusion

Our tracking technique for micro guide wires resulted in a mean TP of 94.8% and mean FP of 5.1 pixels per frame. We conclude that we could develop an accurate automatic tracking technique for micro guide wires in a fluoroscopic sequence, and it would have the potential to adapt clinical fluoroscopic images. In the future, the processing time of the technique needs to be improved and its robustness should be assessed with clinical data.

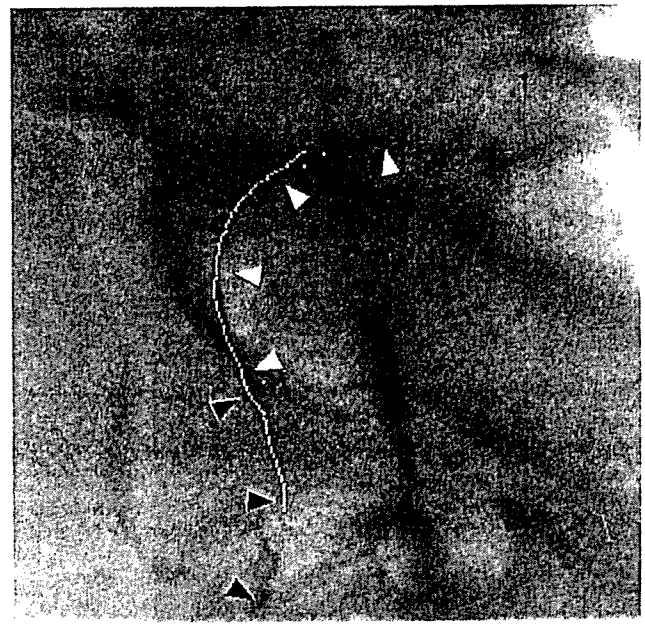

Fig. 7 The frame in which the tracking technique resulted in the worst false positive value. The white triangles indicate this micro guide wire's radio-opaque part, and the black ones indicate its lead section. The gray curvature is the final identified micro guide wire. The tracking technique identified the lead section, making the false positive value worse. The white dots are nodes produced by the double-ring tracking process.

Acknowledgments

We thank Dr. Kenneth R. Hoffmann of the Toshiba Stroke Research Center, University of Buffalo, who gave us much helpful advice.

This research was supported by a grant-in-aid for young scientists (B) (KAKENHI 15790656) of the Ministry of Education, Culture, Sports, Science and Technology of Japan.

References

1) Anxionnat R, Bracard S, Macho J, et al.: 3D angiography. Clinical interest. First applications in interventional neuroradiology. J Neuroradiol, 25(4), 251-262, (1998).
2) Wilson DL, Royston DD, Noble JA, et al.: Determining X-ray Projections for Coil Treatments of Intracranial Aneurysms. IEEE Trans Medical Imaging, 18(10), 973-980, (1999)
3) van Walsum T, Baert SA, and Niessen WJ: Guide wire reconstruction and visualization in 3DRA using Monoplane Fluoroscopic Imaging. IEEE Trans Med Imaging, 24(5), 612-623, (2005).
4) Baert SA, van de Kraats EB, van Walsum T, et al.: Three-dimensional guide-wire reconstruction from biplane image sequences for integrated display in 3-D vasculature. IEEE Trans Med Imaging, 22(10), 1252-1258, (2003).
5) Hoffmann KR, and Esthappan J: Determination of three-dimensional positions of known sparse objects from a single projection. Med Phys, 24(4), 555-564, (1997).
6) Takemura A, Harauchi H, Suzuki M, et al.: An algorithm for mapping the catheter tip position on a fluorograph to the three-dimensional position in magnetic resonance angiography volume data. Phys Med Biol, 48(16), 2697-2711, (2003).
7) Baert SA, Viergever MA, and Niessen WJ: Guide-wire tracking during endovascular interventions. IEEE Trans Med Imaging, 22(8), 965-972, (2003).
8) Baert SA, van Walsum T, and Niessen WJ: Endpoint localization in guide wire tracking during endovascular interventions. Acad Radiol, 10(12), 1424-1432, (2003).
9) Palti-Wasserman D, Brukstein AM, and Beyar RP: Identifying and tracking a guide wire in the coronary arteries during angioplasty from X-ray images. IEEE Trans Biomed Eng, 44(2), 152-164, (1997).
10) Schoonenberg G, Schrijver M, Duan Q, et al.: Adaptive spatial-temporal filtering applied to x-ray fluoroscopy angiography. Proc. SPIE Medical Imaging, 5744, 870-878, (2005).
11) 森　健策，長谷川純一，鳥脇純一郎，他：医用3次元画像における管状画像抽出と気管支内視鏡画像のシミュレーション．3D Image Conference '94，269-274，(1994).
12) 佐野耕一，及川道雄，磯部義明：リージョングローイング法による軟部組織の抽出と3次元表示．Med Imag Tech, 13(3)，189-194，(1995).
13) 関口博之，杉本直三，英保　茂，他：枝単位リージョングローイングによる頭部MRAからの血管抽出．信学論D-II, J87-D-2(1)，126-133, (2004).
14) Chen D, Liang Z, Wax MR, et al.: A novel approach to extract colon lumen from CT images for virtual colonoscopy. IEEE Trans Med Imaging, 19(12), 1220-1226, (2000).
15) Hoffmann KR, Doi K, Chen SH, et al.: Automated tracking and computer reproduction of vessels in DSA images. Invest Radiol, 25(10), 1069-1075, (1990).
16) 林　則夫，真田　茂，鈴木正行，他：頭部MR画像を用いた小脳および脳幹部の自動抽出法の検討．日放技学誌，61(4)，499-505, (2005).

図表の説明

Fig. 1　マイクロガイドワイヤ追跡手法の主な処理のフローチャート

Fig. 2　使用したファントムと透視画像撮影時の配置
画像(a)は頭部ファントムと内頸動脈ファントム，I.I.，X線管の配置を表す．画像(b)は内頸動脈ファントムであり，典型的な内頸動脈の曲線を模している．内部のチューブはシリコンの円筒により固定されている．画像(c)は頭部ファントムで，この実験では透視画像に骨の背景を加えるために使用した．

Fig. 3　double-ring追跡手法の工程
横軸を角度とした二つの同心円上のプロファイルを得て，そのプロファイル同士をAND処理し，一つの2値プロファイルを得る．そのプロファイルから次のノード位置が決められる．その後，内側の円内をバックグラウンドと同じ値で塗りつぶす．

Fig. 4　true positiveとfalse positiveの計算
画像(a)はtrue positive(TP)を表し，画像(b)はfalse positive(FP)を表す．TPは真のマイクロガイドワイヤを構成する画素のうち，認識されたマイクロガイドワイヤから2画素範囲に入る画素数を，真のマイクロガイドワイヤの全画素数で割った百分率である．FPは各フレームごとの真のマイクロガイドワイヤから2画素の範囲に入らないと認識されたマイクロガイドワイヤの画素数である．

Fig. 5　各フレームでのtrue positiveとfalse positiveの結果．グラフ(a)が各フレームにおけるtrue positiveであり，グラフ(b)が各フレームにおけるfalse positiveの結果である．

Fig. 6　結果画像の例．認識されたマイクロガイドワイヤをもと画像に重ね合わせている．白い点はdouble-ring追跡手法によりたどられたマイクロガイドワイヤのノード．灰色の曲線は最終的に認識されたマイクロガイドワイヤの中心線．孤立した白い点は，削除された枝のノードである．

Fig. 7　false positiveが最も悪かったフレームの結果画像
白い三角形は透視画像でのマイクロガイドワイヤの可視部分であり，黒い三角が指し示すのはマイクロガイドワイヤのリード部分である．灰色の曲線は最終的に認識されたマイクロガイドワイヤであり，このフレームでは本手法によりリード部分も認識されたため，false positiveが悪くなった．白い点はdouble-ring追跡手法により得られたノードである．

Microcatheter Tip Enhancement in Fluoroscopy: A Comparison of Techniques

Akihiro Takemura, Ph.D.,[1] Kenneth R. Hoffmann, Ph.D.,[2] Masayuki Suzuki, M.D.,[1] Zhou Wang,[3] Hussain S. Rangwala,[2] Hajime Harauchi,[4] Stephen Rudin, Ph.D.,[2] and Tokuo Umeda, Ph.D.[5]

We compared three techniques for enhancement of microcatheter tips in fluoroscopic images: conventional subtraction technique (CST); averaged image subtraction technique (AIST), which we have developed; and double average filtering (DAF) technique, which uses nonlinear background estimates. A pulsed fluoroscopic image sequence was obtained as a microcatheter was passed through a carotid phantom that was on top of a head phantom. The carotid phantom was a silicone cylinder containing a simulated vessel with the shape and curvatures of the internal carotid artery. The three techniques were applied to the images of the sequence, then the catheter tip was manually identified in each image, and 100 x 100 pixel images, centered at the indicated microcatheter tip positions, were extracted for the evaluations. The signal-to-noise ratio (SNR) was calculated in each of the extracted images from which the mean value of the SNR and its standard deviation (SD) were calculated for each technique. The mean values and the standard deviations were 4.36 (SD 3.40) for CST, 6.34 (SD 3.62) for AIST, and 3.55 (SD 1.27) for DAF. AIST had a higher SNR compared to CST in almost all frames. Although DAF yielded the smallest mean SNR value, it yielded the best SNR in those frames in which the microcatheter tip did not move between frames. We conclude that AIST provides the best SNR for a moving microcatheter tip and that DAF is optimal for a temporarily stationary microcatheter tip.

KEY WORDS: Microcatheter tracking, enhancement technique, subtraction technique, signal-to-noise ratio, comparison of techniques, fluorography, endovascular intervention

INTRODUCTION

The number of endovascular interventions performed for patients with intracranial aneurysms is increasing. These interventions are less invasive than conventional surgery for intracranial aneurysms. In these endovascular interventions, coils, stents, and angioplasty balloons are transported via microcatheters. In such interventions, knowledge of the 3-dimensional (3D) position of the guide wire, the catheter tip, or the microcatheter tip relative to the vascular structures may facilitate the interventions, but determination of the 3D catheter position is difficult because the fluoroscopic image that is usually employed is 2-dimensional and noisy. Magnetic resonance imaging-based navigation systems have been investigated.[1–7] These systems can provide accurate 3D information during intervention, but they also require particular hardware; moreover, special

[1]*From the School of Health Sciences, Faculty of Medicine, Kanazawa University, 5-11-80 Kodatsuno, Kanazawa, 920-0942, Japan.*

[2]*From the Toshiba Stroke Research Center, University at Buffalo (SUNY), 3435 Main St., Buffalo, NY 14214, USA.*

[3]*From the Roswell Park Cancer Institute, Elm & Carlton St., Buffalo, NY 14263, USA.*

[4]*From the School of Allied Health Sciences, Faculty of Medicine, Osaka University, 1-7 Yamadaoka, Suita, 565-0871, Japan.*

[5]*From the School of Allied Health Sciences, Kitasato University, 1-15-1 Kitasato, Sagamihara, Kanagawa, 228-8555, Japan.*

Correspondence to: Akihiro Takemura, Ph.D., School of Health Sciences, Faculty of Medicine, Kanazawa University, 5-11-80 Kodatsuno, Kanazawa, 920-0942, Japan; tel: +81-76-2652538; fax: +81-76-2344366; e-mail: at@mhs.mp.kanazawa-u.ac.jp

Online publication 5 September 2006

doi: 10.1007/s10278-006-0855-6

care and devices are needed because of the magnetic field. Other investigators have proposed methods that provide 3D catheter positions by using devices which transmit electromagnetic signals to allow detection and tracking of a catheter tip in a body in conjunction with conventional x-ray angiography systems.[8,9] Image-based techniques[10] have been proposed for cardiac interventions, which align a catheter model with the catheter image in a single plane C-arm image using the projection Procrustes method.[11] Others have developed techniques to detect guide wires in fluorograms.[12–14]

We are developing an image-based system (the computer-assisted catheter guide system) to help with the navigation of catheters during an intervention for intracranial aneurysms.[15] Specifically, this system will provide image-based 3D catheter locations. However, for full automation and image fusion with this system, the catheter must be detected and tracked automatically and accurately in the images. To facilitate catheter detection, we have developed three catheter enhancement techniques. In this article, we compare these three catheter enhancement techniques in terms of the resulting signal-to-noise ratio (SNR). Evaluations were performed by using a fluoroscopic image sequence of a catheter as it was passed through a carotid phantom.

MATERIALS AND METHODS

A fluoroscopic image sequence of a catheter passing through a carotid phantom was obtained. The images were processed by using three different enhancement techniques: a conventional subtraction technique, a weighted sum of previous images, and a signal extraction technique involving local averages of local pixel values. The quality of the enhancement was evaluated by using the SNR of the resulting signal.

Fluorograms

A digital 1,024 × 1,024 × 12 bit fluoroscopic image sequence of a microcatheter passing through a carotid phantom was acquired by using the CAS-8000 V (Toshiba America Medical Systems, San Francisco, CA, USA) C-arm angiography system. The carotid phantom (Fig. 1a) consisted of a 3-mm-diameter polyethylene tube fixed in a silicone cylinder. The tube was constrained or molded to have the 3D shape and curvatures of a "typical" carotid (as determined by a neuroradiologist). The carotid phantom was positioned on a head phantom (Fig. 1b) to provide images similar to those that would be obtained during interventions, specifically to provide bony structured background in the fluorograms. The carotid phantom was set on the head phantom in a lateral position, and then those phantoms were set on the table of the angiography system. The carotid phantom was filled with a glycerin–water solution that provided smooth movement of the microcatheter. A 2.5 F (0.833 mm) Fastrack-18 Infusion microcatheter (Target, Fremont, CA, USA) was placed in the phantom and drawn back during fluoroscopic acquisition (Fig. 2). The pulsed fluorograms were acquired at 30 frames/second using 94 kVp and 50 mA. The source–surface distance was 100 cm and the magnification was 1.35. The 7-in. image intensifier mode was used (pixel size = 0.174 mm). Total acquisition time was 3.0 s. After acquisition, the 90 images were transferred to our analysis computer.

Techniques

During interventions, the catheter is guided to the site of intervention by observing the progress of the microcatheter tip under fluoroscopy. This microcatheter tip consists of a radiopaque marker with dimensions smaller than 1 mm. The fluorograms used for guidance usually include bone background and are generally noisy because of low dose. To detect and track a microcatheter tip in fluorograms, techniques are required which suppress the bone background and provide good SNR for the catheter tip. In this article, we report on three techniques to achieve these goals: the conventional subtraction technique, the averaged image subtraction technique using temporal averaging we developed, and a double average filtering technique using spatial averaging.

Conventional Subtraction Technique

In the conventional subtraction technique (CST) (one of the simplest techniques to detect object motion between frames), the previous frame is subtracted from the current frame. Microcatheters are darker in fluorograms than background. Thus, the CST is defined as,

$$D_n(x,y) = f_{n-1}(x,y) - f_n(x,y) \quad n = 2,3,4,\ldots \tag{1}$$

$$D_n(x,y) = \begin{cases} 0 & \text{when } D_n(x,y) < 0 \\ D_n(x,y) & \text{otherwise} \end{cases} \tag{2}$$

where $D_n(x, y)$ and $f_n(x, y)$ are respectively the difference image and the image at time point or frame number n. From equation (2), we see that this technique uses a nonlinear process, i.e., if the value of $D_n(x, y)$ is negative, it is set to 0. This nonlinear process should improve SNR by eliminating signals that result from subtraction of high-intensity structures, eg, the catheter tip appearing in the $(n - 1)$ image. Using this technique, stationary structures will be removed, and moving structures will appear as brighter regions.

Averaged Image Subtraction Technique

Fluorograms are usually noisy because of the low dose. In the conventional subtraction technique, the resultant image can be noisier then the original. To reduce increment of noise and

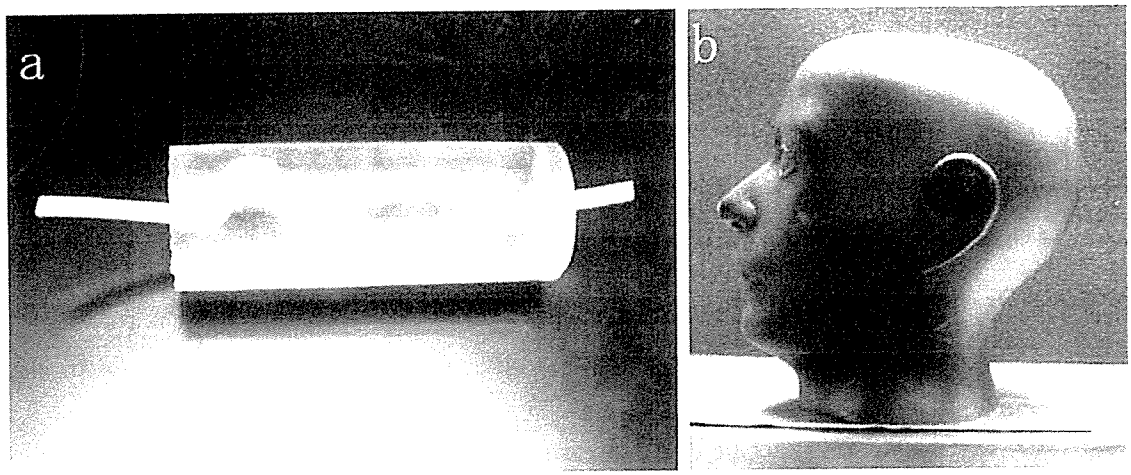

Fig 1. The carotid phantom and the head phantom. (a) A picture of the custom-made carotid phantom. The shape of the centerline of the tube fixed in silicon was based on carotid artery geometries observed by a neuroradiologist. (b) A picture of the head phantom that was used to provide structured background and scatter in the fluorograms.

to improve the SNR of the feature in the resultant image, we have developed a technique that uses an averaged image generated from the frames preceding the current frame and the current frame as a mask image. In this study, three preceding frames were used, thus, the averaged image is defined by the following equation.

$$A_n(x,y) = \frac{1}{4}\sum_{i=n-3}^{n} f_i(x,y), \quad n = 4,5,6,\ldots \tag{3}$$

where $A_n(x, y)$ is the averaged image, n is the frame number, and $f_i(x, y)$ is the original ith image. By using this averaged image as a mask image, the noise in the resultant images is less than that in the images generated using the CST. The equation for this technique in fluorograms in which catheters are darker than the background is thus as follows:

$$m_n(x,y) = A_n(x,y) - f_n(x,y) \qquad n = 4,5,6,\ldots \tag{4}$$

$$m_n(x,y) = \begin{cases} 0 & \text{when } m_n(x,y) < 0 \\ m_n(x,y) & \text{otherwise} \end{cases} \tag{5}$$

where $m_n(x, y)$is a resultant image, $A_n(x, y)$ is an averaged image generated by using equation (4), and $f_n(x, y)$ is the original ith image.

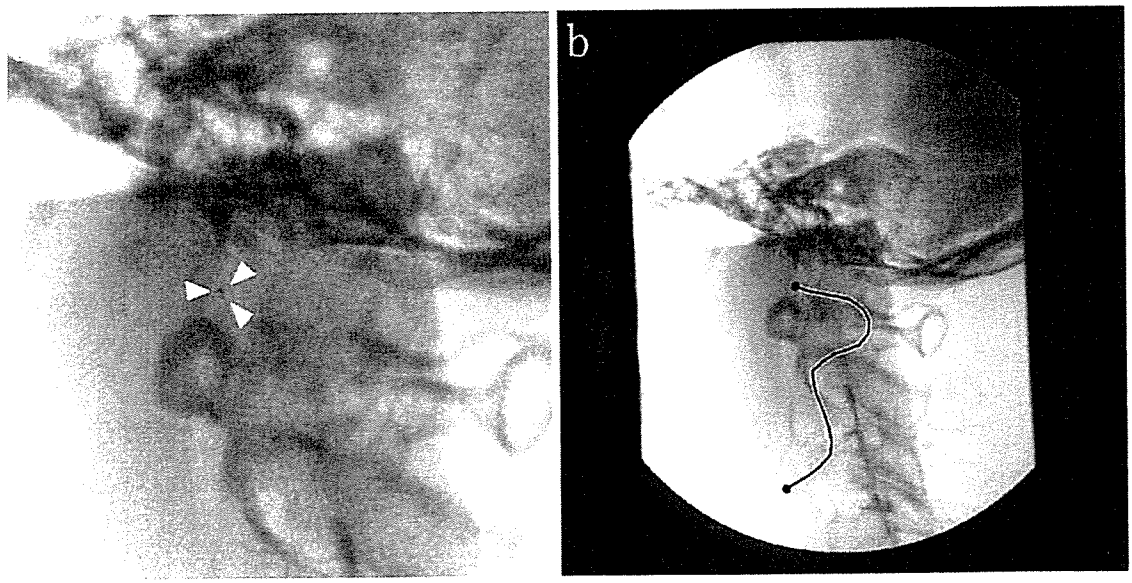

Fig 2. A microcatheter tip in a part of a magnified fluorogram and the path of the microcatheter. (a) White arrows point to the microcatheter tip. (b) The curve represents the path of the microcatheter tip in the sequence of fluorograms.

Note that this subtraction technique employs nonlinear processing similar to that used in the CST and that process could improve the SNR for this technique.

Double Average Filtering Technique

The double average filtering technique (DAF) was proposed as a preprocessing filtering for a vessel tracking technique for the coronary arteries in cine angiograms.[16] The authors indicated that the DAF did not amplify noise and did not generate artifacts that may result from conventional edge enhancement techniques. The double average filtering technique was defined as:

$$M_1(x,y) = \sum_{k=-w}^{w}\sum_{l=-w}^{w} f(x+k, y+l) \tag{6}$$

$$M_2(x,y) = \frac{\sum_{i=-w}^{w}\sum_{j=-w}^{w} f(x+i,y+j)W(x+i,y+j)}{\sum_{i=-w}^{w}\sum_{j=-w}^{w} W(x+i,y+j)} \tag{7}$$

where

$$W(x+i,y-j) = \begin{cases} 1 & \text{when } f(x+i,y-j) < M_1(x,y) \\ 0 & \text{otherwise} \end{cases} \tag{8}$$

$$\tilde{f}(x,y) = \begin{cases} f(x,y) - M_2(x,y) & \text{when } f(x,y) > M_2(x,y) \\ 0 & \text{otherwise} \end{cases} \tag{9}$$

where w is half-width of region of interest (ROI), $f(x, y)$ is the pixel value in the original image at coordinates (x, y), and $\tilde{f}(x, y)$ is the pixel value of final image after filtering by the DAF at coordinates (x, y). $M_1(x, y)$ is the average pixel value of all pixels in ROI, and $M_2(x, y)$ is the average pixel value of all pixels in ROI with pixel value less than $M_1(x, y)$.

Equation (9) is for the image with the signal intensity above the background. Although DAF is not only for such images, we inverted the pixel values in the fluorograms for DAF because the SNR for DAF was calculated by the same equation as for the others (see equation 10).

A size of ROI used in DAF is usually set to twice to triple the size of the feature. We investigated sizes of 5 × 5 up to 21 × 21; 15 × 15 yielded the best results. The size of the marker at the microcatheter tip in the fluorograms was about 5 × 5 pixels.

Measurement of Signal-to-Noise Ratio

To compare the three techniques described above, positions of the catheter tip in the fluorograms were first determined manually. Next, 100 × 100 pixel regions, centered at the indicated microcatheter tip positions were extracted from the fluorograms and processed by using the three techniques. We calculated SNR in each cropped image as:

$$SNR = \frac{\overline{S} - \overline{B}}{SD} \tag{10}$$

where, $\overline{S}$ is the mean pixel value in a 3 × 3 pixel region of 3 × 3 at the center of the extracted fluorograms (at the microcatheter

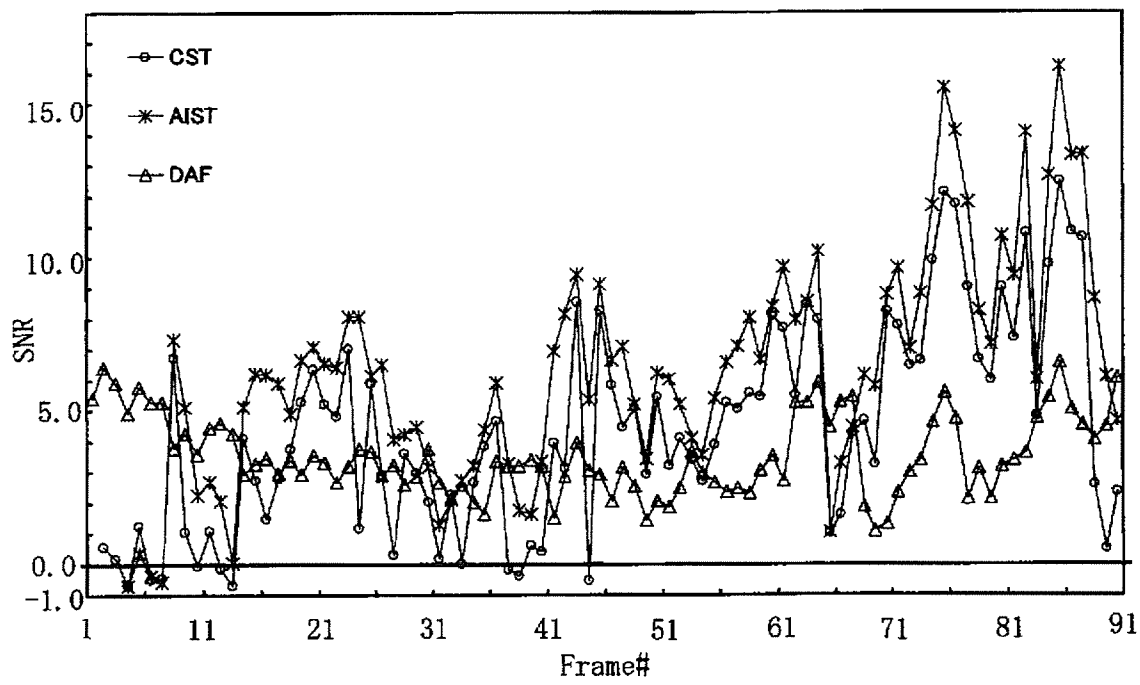

Fig 3. Variation of SNR for the three techniques. The AIST yields the best results, i.e., highest average SNR, whereas the DAF yields the lowest SD of the SNR values.

Table 1. Mean value and standard deviation of Signal-to-Noise Ratio in a sequence of fluoroscopy

Technique	CST	AIST	DAF
Mean value	4.36	6.34	3.55
Standard deviation	3.40	3.62	1.27

tip position), $\overline{B}$ is the mean value of the background, and SD is the standard deviation of background pixel values. A mean value of SNRs was also calculated from all the frames in the image sequence.

RESULTS

Variation in SNRs for each technique is shown in Figure 3, and mean values and SDs of SNRs for the three techniques are shown in Table 1. Based on mean values in Table 1, AIST has the highest overall SNR, and DAF has the lowest SNR but it also yielded the smallest SD. As shown in Figure 3, AIST and CST yielded negative SNR values in some frames, which occur when the catheter tip did not move between frames.

DISCUSSION

SNRs for AIST are similar to those for CST, but AIST showed higher SNRs than CST in almost all frames. It should be noted that AIST and CST are basically motion detectors and yield unreliable results (e.g., negative SNR values) when little or no motion occurs between frames (Fig. 4b and c). However, AIST resulted in fewer frames with negative SNR compared to CST. Thus, AIST appears to provide better enhancement than CST for microcatheter tip tracking in fluorograms.

The mean value of SNRs for DAF is less than those for AIST and CST. However, when the catheter tip does not move, DAF can provide an adequate SNR (Fig. 4d). Thus, AIST and DAF may complement each other in that AIST enhances the moving tip well and DAF enhances the stationary tip well.

When the microcatheter tip is on or near bony background, the tip is enhanced well with AIST and CST, whereas it is obscured with DAF because the local background averages (M_1 and M_2 in Double Average Filtering Technique) have lower pixel values. This is a limitation of DAF.

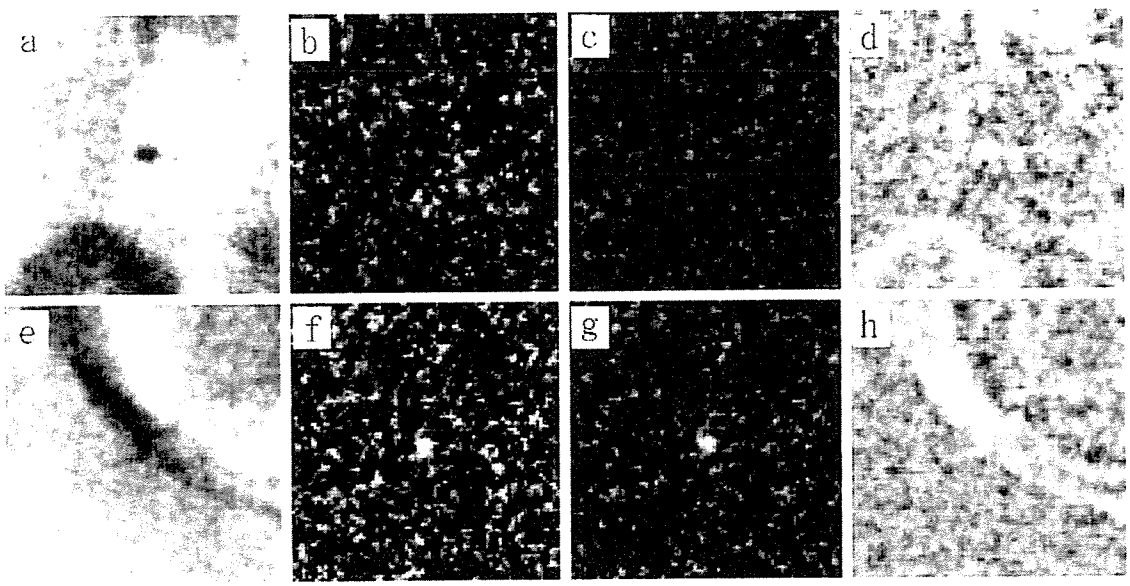

Fig 4. Examples of the original images and the images processed by the three techniques. (a) Original image of frame number seven in the sequential fluorograms. The images resulted from CST (b), AIST (c), and DAF (d). The image of the 7th frame is one of the images in which the catheter tip was not moved, so that the signals of the catheter tip in (b) and (c) have disappeared. (e) Original image of frame number 69 in the sequential fluorograms. The images resulted from CST (f), AIST (g), and DAF (h). The 69th frame is one of the images in which the catheter tip was on a bone edge. The DAF could not isolate the catheter tip signal.

In this study, fluorograms of the head phantom and the carotid phantom were obtained. We believe that addition of the carotid phantom did not affect our results, because each of the techniques estimates and subtracts out the local background. The carotid phantom introduced a slowly varying low-contrast background structure. Thus, the carotid phantom in the fluorograms probably only contributes in increasing the noise near the catheter tip.

CONCLUSIONS

Using SNR, we evaluated three techniques for tracking a microcatheter tip in fluorograms. From our results, we conclude that the averaged image subtraction technique (AIST) is the best of the three techniques for a moving microcatheter tip, and the double average filtering technique is useful for a nonmoving microcatheter tip.

ACKNOWLEDGMENTS

This research supported by a grant-in-aid for young scientists (B) (KAKENHI 15790656) of the Ministry of Education, Culture, Sports, Science, and Technology of Japan and NIH Grant numbers R01 HL52567, R01 EB 02916, R01EB002873, and R01NS43924.

REFERENCES

1. Buecker A, Neuerburg JM, Adam GB, et al.: Real-time MR fluoroscopy for MR-guided iliac artery stent placement. J Magn Reson Imaging 12:616–622, 2000

2. Dion YM, Kadi BEH, Boudoux C, et al.: Endovascular procedures under near-real-time magnetic resonance imaging guidance: an experimental feasibility study. J Vasc Surg 32:1006–1014, 2000

3. Salem RR, Ward BA, Ravikumar TS: A new peripherally implanted subcutaneous permanent central venous access device for patients requiring chemotherapy. J Clin Oncol 11:2181–2185, 1993

4. Quick HH, Ladd ME, Nanz D, et al.: Vascular stents as RF antennas for intravascular MR guidance and imaging. Magn Reson Med 42:738–745, 1999

5. Quick HH, Kuehl H, Kaiser G, et al.: Interventional MR angiography with a floating table. Radiology 229:598–602, 2003

6. Kuehne T, Saeed M, Higgins CB, et al.: Endovascular stents in pulmonary valve and artery in swine: feasibility study of MR imaging-guided deployment and postinterventional assessment. Radiology 226:475–481, 2003

7. Strother CM, Unal O, Frayne R, et al.: Endovascular treatment of experimental canine aneurysms: feasibility with MR imaging guidance. Radiology 215:516–519, 2000

8. Wittkampf FH, Wever EF, Derksen R, et al.: Accuracy of the LocaLisa system in catheter ablation procedures. J Electrocardiol 32 (Suppl 7): 12, 1999

9. Starkhammar H, Bengtsson M, Kay DA: Cath-Finder catheter tracking system: a new device for positioning of central venous catheters. Early experience from implantation of brachial portal systems. Acta Anaesthesiol Scand 34:296–300, 1990

10. Meyer SA, Wolf PD: Registration of three-dimensional cardiac catheter models to single-plane fluoroscopic images. IEEE Trans Biomed Eng 46:1471–1479, 1999

11. Hoffmann KR, Esthappan J: Determination of three-dimensional positions of known sparse objects from a single projection. Med Phys 24:555–564, 1997

12. Baert SAM, van de Kraats EB, van Walsum T, et al.: Three-dimensional guide-wire reconstruction from biplane image sequences for integrated display in 3-D vasculature. IEEE Trans Med Imag 22:1252–1258, 2003

13. Baert SAM, Viergever MA, Niessen WJ: Guide-wire tracking during endovascular interventions. IEEE Trans Med Imag 22:965–972, 2003

14. Palti-Wasserman D, Brukstein AM, Beyar RP: Identifying and tracking a guide wire in the coronary arteries during angioplasty from X-ray images. IEEE Trans Biomed Eng 44:152–164, 1997

15. Takemura A, Harauchi H, Suzuki M, et al.: An algorithm for mapping the catheter tip position on a fluorograph to the three-dimensional position in magnetic resonance angiography volume data. Phys Med Biol 48:2697–2711, 2003

16. Sen A, Lan L, Doi K, et al.: Quantitative evaluation of vessel tracking techniques on coronary angiograms. Med Phys 26:698–706, 1999

JOURNAL OF
JAPANESE SOCIETY OF
NURSING RESEARCH
Volume 29 Number 3 July 2006 ISSN 0285-9262

日本看護研究学会雑誌

[29巻3号]

第32回日本看護研究学会学術集会
—プログラム及び内容要旨—

平成18年度日本看護研究学会総会
—議事事項—

Japanese Society of Nursing Research

112) 日帰り手術における遠隔看護支援システムの構築と有用性の検討

大川明子（名古屋市立大学看護学部）
梅田徳男（北里大学医療衛生学部）
山本晴章（やまもとクリニック）

【目的】
日帰り手術は医療技術の進歩や医療費削減，また患者にとって入院することなく手術を受けられることから，日常生活への影響が少なく，治療費も安くなるなどの利点があるため，希望者が増加している。しかしこれまでの術前・術後の管理については患者や家族に委ねられる部分が多く，術前・術後の説明もコーディネーターが電話相談で対応しているのが現状である。
そこで本研究では日帰り手術における遠隔看護支援実験システムを構築し，その有用性と課題とを検討する。
【方法】
在宅側PCと施設側PCとをインターネット回線で接続した双方向通信実験システムを構築する。構築システムは，術前と術後とに，在宅患者や家族が必要とする準備やセルフケア内容に関することや，術前用には日帰り手術計画画面を作成して手術内容に関することを理解できるようにする。その際，手術室の案内や手術担当者の紹介をビデオや写真画像に取り込み，映像で見られるようにする。また患者の理解度を把握するため，説明に対する理解内容に関するアンケートの回答をWebから実施できる入力画面を作成する。次に，手術当日に関する内容画面と，術後の合併症予防に関する日常生活の留意事項画面を作成する。また電話相談に替わるものとして，構築システムにカメラ・ボイスシステムを装備する。
直接被験者を介した研究ではなく，在宅側と施設側とを想定したシステム間をデジタル模擬回線で接続し，研究者間の実験としたことから本研究における倫理的な配慮についての検討はしなかった。
【結果】
双方向実験システムであることから綿密な確認と把握をすることができ，術前・術後の管理支援システムとなった。また映像を用いて案内・説明したことにより，視覚から患者や家族がなすべきことを把握できるようにした。さらに説明内容の理解度に関するアンケートを実施することにより，対象者の把握の程度を知ることができた。
【考察】
これまで周手術期における看護介入の大半は，在宅での自己管理となっている。日帰り手術は低侵襲であるが，手術を受ける患者や家族にとっては不安であり，自己判断が必要な場面が多い。本構築遠隔看護支援システムは，必要なときに情報を得ることができ，相談することができることから，患者や家族の精神的援助にもつながると考えられる。今後はフィールドテストを行い，患者の利用評価を調査していく必要がある。

113) クリティカルケアに携わる看護師の職務満足度と関連因子

川上千普美（九州大学医学部保健学科）
松岡　綠（大分大学医学部看護学科）

【目的】
クリティカルケアに携わる看護師の職務満足度とその関連因子を明らかにすること。
【方法】
九州北部にある26施設の救急外来，救命救急センター，ICU，CCUに勤務する看護職者807名を対象とし，郵送法による質問紙調査を実施した。対象者には研究の主旨や参加の自由，匿名性の保持等を書面で説明し，倫理的配慮を行った。
調査内容は1）職務満足度（看護職，現所属），2）属性（性別，年齢，看護師経験年数，現所属の勤務年数，役割，教育課程），3）社会的支援（上司，同僚，家族/友人），4）自己効力（一般性セルフエフィカシー尺度），5）バーンアウト（Pines Burnout尺度）で構成し，分析は，Mann-Whitney U検定，Kruskal-Wallis検定，spearmanの積率相関係数，重回帰分析を用いた。
【結果】
652名の回答（回収率80.8%）を得たうち，608名を分析対象とした。男性38名，女性566名，平均年齢31.5 ± 7.6歳であった。看護師経験年数の平均は9.6 ± 7.3年，現所属の勤務年数は平均3.4 ± 3.1年，役割ではスタッフが231名，リーダー293名，副看護師長・師長69名で，教育課程では専門学校が467名，短大75名，大学以上が31名であった。
看護職および所属部署に対する満足度と有意差が認められたのは，役割，教育課程であった。有意な相関があった項目については表1に示した。性別での有意差，年齢，看護師経験年数との相関はなかった。更に，看護職に対する満足度に影響していたのは，バーンアウト，自己効力，上司の支援，役割で，所属部署に対する満足度では，バーンアウト，上司の支援，教育課程，役割が有意な変数であった（表2）。
【考察】
バーンアウトと上司の支援があること，責任ある役割を担っていることは，共通して職務満足度に関連していた。職場環境を考える上で，メンタルヘルスの支援体制について検討し，強化していく必要性が示唆された。また，看護師の背景にも着目しながら役割を明確化し，それぞれの立場での課題や目標達成が可能となるように支援していく重要であると思われる。

表1　職務満足度との相関関係

(NS: No Significant, $^{**}p<.01$, $^{*}p<.05$)

	−社会的支援− 上司	同僚	家族/友人	自己効力	バーンアウト	現所属の勤務年数
看護職に対する満足度	.25**	.21**	.15**	.35**	−.34**	NS
所属部署に対する満足度	.38**	.22**	.14**	.19**	−.43**	.08*

表2　職務満足度の要因分析

（β：標準偏回帰係数，R：決定係数，$^{***}p<.001$，$^{**}p<.01$，$^{*}p<.05$）

従属変数	看護職に対する満足度		所属部署に対する満足度	
独立変数	バーンアウト	$\beta=-.24^{***}$	バーンアウト	$\beta=-.34^{***}$
	自己効力	$\beta=.22^{***}$	上司の支援	$\beta=.29^{***}$
	上司の支援	$\beta=.15^{***}$	教育課程	$\beta=-.11^{**}$
	役割	$\beta=.08^{*}$	役割	$\beta=.09^{*}$
	R=.46	R^2=.21	R=.53	R^2=.28

164) 在宅患者を対象とした訪問看護支援システムの構築

梅田徳男（北里大学医療衛生学部）
大川明子（名古屋市立大学看護学部）
山本晴章（やまもとクリニック）

【はじめに】
患者の多くは，できるだけ地域・家庭において日常生活を送ることを望んでいる。また，60歳以上の半数が自宅での療養を希望しているため，訪問看護の需要が高まっている。
【目的】
本研究では訪問看護を支援する実験システムを構築する。システム構築に当たり，在宅患者に安心感を与えられるシステムとすること，操作が簡便であること，とする。また，訪問看護師などの医療スタッフにはシステム操作性の利便性と共に作業負担の軽減を目指したシステムとする。
【方法】
実験システムは在宅患者側システム，訪問看護システムを含む医療機関側システムとする。システムのソフトウエアの管理はそのメンテナンスも含めて全て医療機関側で行う。構築システムへのLoginには在宅患者，看護・介護者，医師の3段階の資格を設け，閲覧・入力可能な医療情報を区別する。また，カメラ・ボイスシステムをシステムに装備することで，在宅患者の褥瘡状態を医療機関側に伝送し，その場で相談できるようにする。さらに，在宅患者やその家族の負担を軽減するためにデータ入力操作は簡便となるような配慮や訪問看護師の報告書作成の支援をも行う。
【結果・考察】
Login資格を3段階にすることで，在宅患者宅でも構築システムを利用して訪問看護師などの医療従事者は，医療機関側でのシステム利用と同じ操作で当該在宅患者の全情報が閲覧でき，情報入力も可能となった。また，カメラ・ボイスシステムを装備したことで，在宅患者は①訪問看護師と疑似対面相談が可能となったこと，訪問看護師は②患者宅を訪問することなく相談に対応可能となったこと，③在宅患者の状態が把握できるようになったこと，訪問看護師が患者宅を訪問した場合には，④褥瘡の様子を写真撮影し，担当医とその場で相談できるようになった。これらにより，在宅患者の安心感が増加すると予想され，訪問看護師も担当医と相談することでセカンドオピニオンが得られるようになった。さらに，⑤報告書作成に際してもこれら在宅患者の医療情報が報告書に転用できるために，在宅患者に向き合う時間が増加した。
以上のシステム開発時にはダミーデータを利用するため，倫理面における新たな問題は発生しないが，システム試行に際しては在宅患者の人権およびプライバシーに十分配慮し同意を得て行う。
【まとめ】
在宅患者は医療従事者と疑似面談を行えるため，また訪問看護師はいつでも担当医と相談できるため，安心感が増した。また，在宅患者データ入力が簡便なので，在宅患者や訪問看護師の負担を軽減できた。今後はフィールドテストの実施を行う予定である。
最後に本研究の一部は厚労科研（H16－医療－021），文科省科研（課題番号15209022）の補助を受けた。

165) 介護支援専門員支援方法としてのグループスーパービジョンの有効性の検討

若林たけ子，竹本三重子，小池　敦（三重県立看護大学）
川口ちづる（三重大学大学院修士課程）

【目的】
本研究では，制度化された支援体制がない現状で働く介護支援専門員を対象に，GSV（グループスーパービジョン）を実施し，介護支援専門員に対する支援方法としての有効性について明らかにする。
【研究方法】
ＧＳＶ参画に同意が得られた介護支援専門員（看護師と他職種者）11名のうち，バイザーを除いて3回以上セッションに参加できた7名を対象とした。その中でバイジー，メンバーの役割を決定し，奥川グループ・スーパービジョンモデルを参考に，事例を用いたＧＳＶを，平成17年9月から12月まで4回実施した。島内のケアマネジメント業務調査票（9領域69項目）を用いて，GSV実施前と実施後の自己評価（「できない1」から「できる4」の4段階）の比較と，GSVに対する評価の記述内容を質的に分析した。倫理的配慮は，研究趣旨，プライバシーの保護，調査目的以外には使用しないことなどを明記した文書でもって協力依頼を行い，三重県立看護大学研究倫理委員会の承認を得た。
【結果】
ケアマネジメント業務調査票における全体の平均得点は，前が3.29点，後が3.42点で＋0.13であった。役割別ではバイジーが3.08点→3.47点（＋0.39）と高い上昇を示し，メンバーは3.66点→3.49点（－0.17）と僅かの低下を示した。バイジーの得点は9領域中8領域で全て上昇し，特に「事務管理」，「アセスメント」，「調整と同意」が，「あまりできない」から「概ねできる」に変化した。一方メンバーは「評価」の（－0.55）を始め他7領域で，0.12から0.23の（－）を示した。自己評価において「できない」「あまりできない」と回答した平均項目数は，バイジーが16.25→5.75に減少し，メンバーは2.0→2.6に増加した。バイジーの得点上昇率を項目別で見ると，「事務管理」100%，「評価」83.3%，「調整と同意」81.8%，「計画作成」77.8%，「開始準備」75%，「アセスメント」63.6%の順であった。ＧＳＶの評価では，参加者全員が自分自身の気づきをあげ，今後の取り組みに生かせると答えた。特にバイジーは，振り返る事とメンバーの質問に答えていくことで，不透明だったものが透明化し，今後の方向性が見えてきたと答えた。
【考察】
バイジーになった人は業務に少し自信がなく，より積極的にバイジーになろうとしていたことが伺える。バイジーとして積極的に事例を報告することで，自分の抱えている問題が明確化し，業務に自信をもてるようになったことが，得点の上昇率に繋がったものと考える。またメンバーは自己評価をより正確にできるようになったものと考える。以上から介護支援専門員支援方法としてのＧＳＶは，業務における質的効果とともに，介護支援専門員への内的支援としても有効性が示唆された。

COMPUTER METHODS AND PROGRAMS IN BIOMEDICINE 81 (2006) 197–202

ELSEVIER

journal homepage: www.intl.elsevierhealth.com/journals/cmpb

Design and development of a secure DICOM-Network Attached Server

Hidenobu Tachibana, Masahiko Omatsu, Ko Higuchi, Tokuo Umeda*

Medical Image Engineering, Kitasato University, Graduate School of Medical Sciences, 1-15-1 Kitasato, Sagamihara, Kanagawa 228-8555, Japan

ARTICLE INFO

Article history:
Received 1 November 2003
Received in revised form 6 June 2004
Accepted 22 October 2004

Keywords:
Teleradiology
Web-based system
DICOM
INTERNET
DICOM-NAS

ABSTRACT

It is not easy to connect a web-based server with an existing DICOM server, and using a web-based server on the INTERNET has risks. In this study, we designed and developed the secure DICOM-Network Attached Server (DICOM-NAS) through which the DICOM server in a hospital-Local Area Network (LAN) was connected to the INTERNET. After receiving a Client's image export request, the DICOM-NAS sent it to the DICOM server with DICOM protocol. The server then provided DICOM images to the DICOM-NAS, which transferred them to the Client using HTTP. The DICOM-NAS plays an important role between DICOM protocol and HTTP, and only temporarily stores the requested images. The DICOM server keeps all of the original DICOM images. When unwanted outsiders attempt to get into the DICOM-NAS, they cannot access any medical images because these images are not stored in the DICOM-NAS. Therefore, the DICOM-NAS does not require large storage, but can greatly improve information security.

1. Introduction

In recent years, many hospitals have installed high-tech medical equipment, including Computed Radiology (CR), Computed Tomography (CT), and Magnetic Resonance Imaging (MRI) [1]. Researchers and developers have attempted to combine this equipment with information technology (IT) to improve the quality of medical care. Web-based servers, which have enabled us to display patients' medical images on computers using Internet Explorer, have been especially developed. This allows medical physicians and other researchers to easily share and view these medical images anywhere when needed. However, the use of web-based servers also brings many problems [2–13].

Since most servers were originally designed for vender-customized DICOM servers, their versatilities are not very good. Therefore, users must install a web-based server combined with a particular DICOM server for medical use. This is sometimes not feasible because of technical and financial reasons. On the other hand, in order to distribute the medical images, patients' information must be stored in the servers at all times. Therefore, the misusage risk of patients' information becomes higher.

The present study developed a web-based server called the DICOM-Network Attached Server (DICOM-NAS), which can be easily installed and adjusted to DICOM protocol and HTTP. The DICOM servers in a hospital-LAN are connected to the INTERNET through the DICOM-NAS, and the patients' medical images and information are only kept temporarily in the DICOM-NAS when eligible Clients need them. Since the patients' medical images are not stored there at all times, it greatly improves information security.

* *Corresponding author.* Tel.: +81 42 778 9565; fax: +81 42 778 9565.
E-mail address: tatibana@umeken3.ahs.kitasato-u.ac.jp (H. Tachibana).
0169-2607/$ – see front matter © 2006 Published by Elsevier Ireland Ltd.
doi:10.1016/j.cmpb.2005.11.015

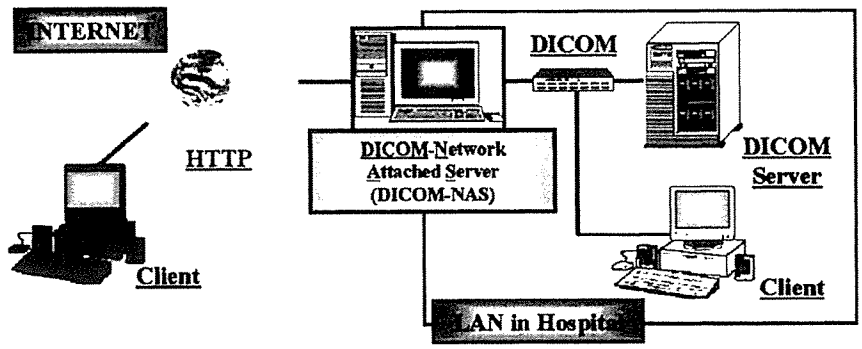

Fig. 1 – Scheme of DICOM-Network Attached Server.

2. DICOM-Network Attached Server

2.1. *Scheme of DICOM-NAS*

The DICOM-NAS scheme is illustrated in Fig. 1. It communicates with the DICOM server by using the DICOM protocol when it is attached to the Local Area Network (LAN). An IP address, AE title, host name, and port number were assigned to the DICOM-NAS. In order to view the DICOM images, the Client can use the browser in any computer to connect to the LAN, the INTERNET, and then to the DICOM-NAS.

2.2. *System configuration of DICOM-NAS and data flow*

Fig. 2 demonstrates the system configuration of the DICOM-NAS and the data flow. The DICOM-NAS can work with Internet Information Server (IIS) 5.0 on Microsoft Windows 2000 or XP and consists of Java Applets, Java Servlets, and DCMTK. The Java Servlets work with application servers Tomcat 4.0.1 and IIS 5.0 to provide a highly reliable, manageable, and scalable web application infrastructure for all versions of Windows 2000 and XP. The IIS can increase website and application availability and lower the system administration costs. Java Servlets provide a component-based and platform-independent method for building web-based applications without CGI program performance limitations. Java Servlets can access the entire Java API family, including JDBC API, to access enterprise databases and a library of HTTP-specific calls. They have all of the benefits of mature Java language, including portability, performance, reusability, and crash protection. Tomcat 4.0.1 is the servlet container that can improve performance and memory efficiency. DCMTK [14] is a collection of libraries and applications that implement large parts of the DICOM standard. It includes software for examining, constructing, and converting DICOM image files, as well as sending and receiving images over a network connection.

In this DICOM-NAS system, the Java Applets are the interfaces between the Client and the Java Servlets. The Java Servlets communicate with the DCMTK and the Diagnosis report database based on the information obtained from the Java Applets. The DICOM-NAS communicates with the DICOM servers using two applications, including DCMTK, which has the C-FIND and C-MOVE functions.

When a Client wishes to access the medical images of a patient, the Client should first connect to the DICOM-NAS using Internet Explorer and request a patient name or a patient name list, which is stored in the DICOM server. After receiving the request, the DICOM-NAS generates query keys related to the request and sends them to the DICOM server

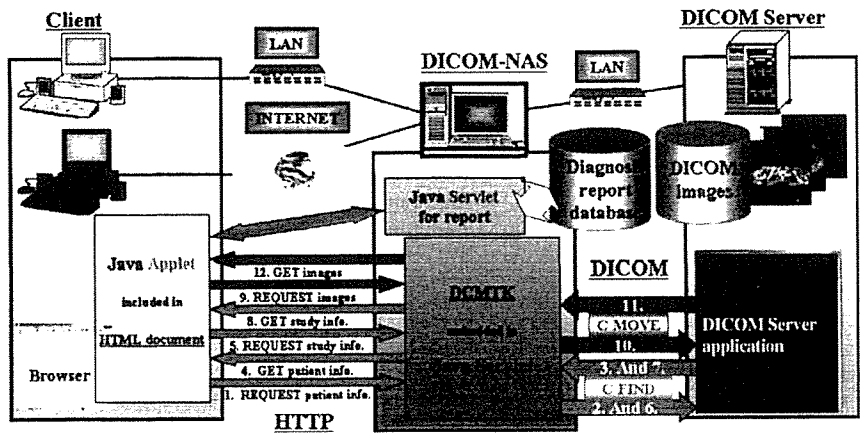

Fig. 2 – System configuration of DICOM-NAS, and data flow after downloading Java Applet that have the functions of Query/Retrieve and display of DICOM images from DICOM-NAS.